International Journal of Nanomedicine

Dovepress
open access to scientific and medical research

Open Access Full Text Article

ORIGINAL RESEARCH

Malachite green-conjugated multi-walled carbon nanotubes potentiate antimicrobial photodynamic inactivation of planktonic cells and biofilms of *Pseudomonas aeruginosa* and *Staphylococcus aureus*

This article was published in the following Dove Press journal:
International Journal of Nanomedicine

VT Anju[1]
Parasuraman Paramanantham[1]
Busi Siddhardha[1]
SB Sruthil Lal[2]
Alok Sharan[2]
Abdullah A Alyousef[3]
Mohammed Arshad[3]
Asad Syed[4]

[1]Department of Microbiology, School of Life Sciences, Pondicherry University, Puducherry 605014, India; [2]Department of Physics, School of Physical, Chemical & Applied Sciences, Pondicherry University, Puducherry 605014, India; [3]Microbiology Research Group, Department of Clinical Laboratory Sciences, College of Applied Medical Sciences, King Saud University, Riyadh 11433, Saudi Arabia; [4]Department of Botany and Microbiology, College of Science, King Saud University, Riyadh 11451, Saudi Arabia

Purpose: Infections associated with medical devices that are caused by biofilms remain a considerable challenge for health care systems owing to their multidrug resistance patterns. Biofilms of *Pseudomonas aeruginosa* and *Staphylococcus aureus* can result in life-threatening situations which are tough to eliminate by traditional methods. Antimicrobial photodynamic inactivation (aPDT) constitutes an alternative method of killing deadly pathogens and their biofilms using reactive oxygen species (ROS). This study investigated the efficacy of enhanced in vitro aPDT of *P. aeruginosa* and *S. aureus* using malachite green conjugated to carboxyl-functionalized multi-walled carbon nanotubes (MGCNT). Both the planktonic cells and biofilms of test bacteria were demonstrated to be susceptible to the MGCNT conjugate. These MGCNT conjugates may thus be employed as a facile strategy for designing antibacterial and anti-biofilm coatings to prevent the infections associated with medical devices.

Methods: Conjugation of the cationic dye malachite green to carbon nanotube was studied by UV-visible spectroscopy, high-resolution transmission electron microscopy, and Fourier transform infrared spectrometry. *P. aeruginosa* and *S. aureus* photodestruction were studied using MGCNT conjugate irradiated for 3 mins with a red laser of wavelength 660 nm and radiant exposure of 58.49 J cm^{-2}.

Results: Upon MGCNT treatment, *S. aureus* and *P. aeruginosa* were reduced by 5.16 and 5.55 log_{10} , respectively. Compared to free dye, treatment with MGCNT afforded improved phototoxicity against test bacteria, concomitant with greater ROS production. The results revealed improved biofilm inhibition, exopolysaccharide inhibition, and reduced cell viability in test bacteria treated with MGCNT conjugate. *P. aeruginosa* and *S. aureus* biofilms were considerably reduced to 60.20±2.48% and 67.59±3.53%, respectively. Enhanced relative MGCNT phototoxicity in test bacteria was confirmed using confocal laser scanning microscopy.

Conclusion: The findings indicated that MGCNT conjugate could be useful to eliminate the biofilms formed on medical devices by *S. aureus* and *P. aeruginosa.*

Keywords: aPDT, MGCNT, Biofilms, reactive oxygen species, CLSM

Correspondence: Busi Siddhardha
Department of Microbiology, School of Life Sciences, Pondicherry University, Puducherry 605014, India
Tel +91 959 776 1788
Email siddhardha.busi@gmail.com

Introduction

In contrast to the enhanced life expectancy associated with advanced health care systems, the complicated infections caused by device-associated and surgical site

infections remain a significant public health threat. Notably, such infections, owing to multidrug-resistant pathogens, respectively, account for nearly 26% and 22% of all health care-associated infections.[1] Moreover, these medical device-associated infections impose large financial burdens on health care services and result in increased patient morbidity and mortality.[2] To address these issues, antimicrobial agents discovered to date have been exploited in clinical treatments as therapeutic agents against microbial infections.[3]

Microorganisms such as Gram-positive *Corynebacteria, Staphylococcus aureus, Enterococci*, along with coagulase-negative *Staphylococci* Gram-negative organisms including *Pseudomonas, Serratia*, and *Acinetobacter* species are most frequently associated with device-associated chronic infections.[4] Resistant strains may develop new mechanisms over days or months that allow bacteria to be recalcitrant toward the effects of a wide spectrum of antibiotics. The immense challenge afforded by antimicrobial resistant strains is that they diminish drug efficacy over time.[5] The mechanism of antibiotic resistance may be innate or acquired. Some strains of bacteria are innately resistant to various classes of antibiotics whereas others acquire genes for enzymes that degrade antimicrobial agents or may acquire efflux pumps to extrude these agents before they reach the target site. Bacteria may also acquire antibiotic-resistant genes by alternating the metabolic pathway by itself or through new mutations.[6]

The infections caused by resistant strains are mainly due to biofilm formation, which accounts for up to 80% of the total infections. Bacterial biofilms are defined as a well organized and structured community comprised of bacterial cells protected from the outside environment through the production of an exopolysaccharide (EPS) matrix. This EPS production enables the cells to attach to inert or living surfaces for survival and further establishment. Formation of biofilms thus constitutes an essential factor for survival in extreme environments, as well as a phenomenon observed in clinical specimens.[7] However, bacterial biofilms are difficult to eliminate by antimicrobial agents or through other methods and also show resistance toward a wide range of antibiotics and biocides.

Therefore, it is essential to take firm steps to fight against biofilms and associated infections. In particular, antimicrobial photodynamic therapy (aPDT) has emerged as a potential candidate to eliminate biofilms. aPDT includes three components: nontoxic photosensitizers (PS), light of a particular wavelength, and oxygen present in the environment, which lead to the generation of cytotoxic reactive oxygen species (ROS) upon illumination.[8] aPDT eliminates the possibility of development of resistant strains without causing genotoxic or mutagenic effects. Among several groups of photosensitizers, malachite green (MG), a cationic dye belonging to the triarylmethane family, has been used in photosensitization studies. MG can cross the cell walls of both Gram-negative and positive bacteria to exhibit broad spectrum antibacterial action.[9] For example, MG has demonstrated phototoxicity against a number of bacteria and fungi including *S. aureus, Staphylococcus epidermidis, Staphylococcus schleiferi, Staphylococcus capitis, Staphylococcus haemolyticus, Staphylococcus lentus. Enterobacter cloacae, Klebsiella pneumoniae, Klebsiella oxytoca, Escherichia coli, Candida albicans, Candida tropicalis Candida parapsilosis, Candida krusei*, and *Candida glabrata*.[10] Specifically in previous studies the phototoxicity of MG against *S. aureus* biofilms was effected by ROS other than singlet oxygen.[11]

Drug delivery vehicles have attracted increased interest in aPDT as most of the known photosensitizers tend to from inactive aggregates and are insoluble. In particular, the advancement in nanotechnology has provided various nanoplatforms for the enhanced and effective delivery of dye to target cells.[12] Recently, nanoplatforms have been designed to enhance drug delivery to target sites through the selective and triggered adsorption and release of drugs.[13,14] Among several carbon nanostructures, carbon nanotubes (CNTs) are recognized for their antimicrobial activities mediated by photo-generated ROS.[15] CNTs are reported to be an effective material for immobilization of antimicrobial agents and their functionalization renders them potent candidates for enhanced aPDT.[16] The physical and chemical properties of CNTs such as their length, diameter, electronic structure, residual catalyst, surface chemistry, and functional groups, along with specific functionalization influences their antibacterial and drug delivery activities.[15] Owing to their sp^2-hybridized carbon surfaces and large surface area, CNTs have a high-loading capacity (LC) for the delivery of several payloads.[17] Researchers have reported CNTs conjugated with rose bengal for maximum antimicrobial photodynamic destruction of *E. coli* biofilms, wherein CNTs act as a dye carrier.[18] In another study, single-walled-CNT-aminoporphyrin conjugates were synthesized for the efficient photodynamic inactivation of Gram-positive bacteria.[19] This study was aimed to potentially enhance

the phototoxic effects of MG conjugated to carboxy-functionalized multi-walled CNTs (MWCNTs) against *Pseudomonas aeruginosa* PA01 and *S. aureus* were examined.

Experimental

Chemicals

Carboxyl-functionalized MWCNTs (length, 1.5 µm; diameter, 9.5 nm) were purchased from Sigma-Aldrich, USA. MG was procured from Himedia Laboratories Private Limited, India.

Bacterial strains and growth media

The Gram-negative bacterium *P. aeruginosa* PA01, a gift of Dr. E. Peter Greenberg (Department of Microbiology, University of Washington and School of Medicine), and Gram-positive bacterium *S. aureus* MCC 2408 (Microbial Culture Collection, National Centre for Microbial Resource, Pune, India) were used as test microorganisms. *S. aureus* and *P. aeruginosa* were selected owing to their ability to form biofilms on medical devices causing healthcare-associated chronic infections.[2] Bacteria were aerobically grown in Luria Bertani (LB) broth at 37°C for 24 hrs in shaking conditions for all assays. Bacterial culture of 1.5×10^8 colony forming units (CFU/mL) with a McFarland standard of 0.5 was employed for all experiments.

Preparation of MGCNT conjugate

The synthesis of MG conjugated to CNT was performed according to the method described previously.[19] MG (1.25 mg) was added to 10 mL of deionized water containing 5 mg of CNT, sonicated at room temperature for 15 mins, and magnetically stirred for 24 hrs. The solution was centrifuged for 10 mins at 10,000 rpm after magnetic stirring. The pellet was collected and washed three times with deionized water, and dried at 55°C. The powder of the MGCNT conjugate was subjected to various assays to determine the spectroscopic measurements and biological activities.

Characterization of MGCNTs

UV-visible absorbance of MGCNTs was recorded using a UV-visible spectrophotometer (UV 3600 Plus, Shimadzu-Japan) in a wavelength range of 250–800 nm. A high-resolution transmission electron microscope (HRTEM) (HITACHI H-8100, Japan) was used for the determination of particle size and to study the structure of MGCNTs with an accelerating voltage of 200 kV. The functional groups present in the MGCNT conjugate were recorded using a Fourier Transform Infrared Spectrometer (FTIR) (Nicolet-6700, Thermo-USA) in the range of 400–4000 cm^{-1} .

LC of MG and entrapment efficiency (EE) of CNTs

The LC and EE were measured as follows.[20] Approximately 2 mg of MGCNT conjugate was added to absolute ethanol (2 mL) and vortexed for 2 mins. The obtained solution was centrifuged for 20 mins at 10,000 rpm to enable the complete release of MG. The optical density of supernatant containing MG was read at 615 nm to determine the loading and EE. Loading and EE were determined using the following equations:

$$\text{Loading capacity} = (W1/W2)\times 100\%$$

$$\text{Entrapment efficiency} = (W1/W3)\times 100\%$$

where W1 is the amount of dye (MG) in MGCNT, W2 is the amount of MWCNTs used for the conjugation experiment, and W3 is the gross weight of MG used for conjugation experiment.

Dye release kinetics

The release of dye was examined at room temperature using the following method with slight modifications.[15] Approximately 1 mg of MGCNTs was dispersed in 1 mL of phosphate-buffered saline (PBS:pH 7.4). The resulting solution was centrifuged at every 30 mins and replaced with fresh PBS for further release of dye after collecting the supernatant. The release profile of MG was measured at each time interval by determining the absorbance of the supernatant at 615 nm. The amount of the MG released was estimated using a standard calibration curve for MG. The release study data were subjected to the evaluation of release kinetics by fitting to a Korsmeyer–Peppas kinetics model, which was analyzed as follows:

$$F = (Mt/M) = Ktn$$

where: F=the fraction of drug released at time t. Mt=the amount of drug released at time t, M=the total amount of drug in dosage form, K=the kinetic constant, and n=the release exponent. Correlation coefficient values (R^2) were calculated for the Korsmeyer–Peppas kinetics model.

Uptake of MG by *S. aureus* and *P. aeruginosa*

About 2 mL of overnight bacterial test cultures () with a McFarland standard of 0.5 was treated with 2 mg of free MG and MGCNT conjugate.[21] The solution was centrifuged at 10,000 rpm for 10 mins at different time intervals (30, 60, 90, 120, 150, and 180 mins), which allowed the cells to settle at the bottom. The bacterial pellet containing internalized dye was treated with 1 mL of methanol for 1 hr at room temperature and centrifuged at 10,000 rpm for 10 mins. The methanol-extracted supernatant containing dye was collected. The amount of dye bound to the bacterial cells was measured spectrophotometrically at 615 nm. The percentage of dye uptake was expressed as follows:

% Uptake of MG=[MG present in the dissolved pellet/total amount of MG used for conjugation]*100

Photosensitizer and light source

The photosensitizer used was MG. A stock solution of MG (10 mg/mL) was prepared and stored in the dark. The photosensitization of samples was performed using a red diode laser of 125 mW with an emission wavelength of 660 nm.[22] The photosensitization of samples was carried out in a 96 well microtiter plate containing circular bottom wells. The irradiated area was calculated as πr^2, where r = radius of the well, ie, 0.35 cm. The radiant exposure was calculated using the following equations:

$$\text{Radiant exposure} = \text{Power density} \times \text{Exposure time}$$

$$\text{Power density(P.D.)} = \text{P(W)/A}\left(\text{cm}^2\right)$$

where P= the radiant flux of the laser used for exposure in Watts (W) and A = the irradiated area in cm^2 (πr^2).[18]

The radiant exposure of the laser was measured according to the radiant flux and time of irradiation of samples. The radiant exposure was measured as 58.49 J cm^{-2}. The bacteria were treated with MG (50 µg/mL)[23] and MGCNTs (484.82 µg/mL) such that the final concentration of MG present in the conjugate was equal to 50 µg/mL. The optimization of exposure time for maximum photoinactivation in test bacteria was carried out using different irradiation times. The concentration of CNTs used for assays was fixed at 434.82 µg/mL. which is similar to the concentration of CNTs present in MGCNTs. The test samples were irradiated for 3 mins after pre-incubation in the dark (3 hrs). The test samples were distributed as eight different groups (Table 1).

In vitro photosensitization of samples

Overnight test bacterial cultures grown in LB broth were adjusted to a McFarland standard of 0.5. Each bacterial culture (100 µL) was dispensed into 96-well multitier plates and treated with CNTs, MG, or MGCNTs at respective concentrations of 434.82, 50, and 484.82 µg/mL. All eight samples mentioned in Table 1 were treated and irradiated as described above. After the pre-incubation of all samples in the dark for 3 hrs, samples 2, 4, 6, and 8 were photoactivated for 0, 3, 5, and 10 mins using a red laser of 660 nm wavelength (58.49 J/cm^{-2}). Samples 1, 3, 5, and 7 were maintained in dark conditions. Light exposed and unexposed samples were serially diluted. The serial dilutions were plated on LB agar and incubated for 24 hrs at 37°C. The $\log_{10}$ reductions in the growth of planktonic cells were calculated by comparison with the CFU/mL of control and treated samples. All the experiments were performed in triplicates.

Detection of intracellular ROS

Intracellular measurement of ROS was performed using 2′,7′-dichlorofluorescein diacetate (DCFH-DA),[24] which can pass through the bacterial cell membrane and produce

Table 1 Different bacterial treatments and irradiation groups used in the study

Sample number	Abbreviation used	Treatment
Sample 1	Control (L^-)	Bacterial samples incubated in the dark and not treated with CNTs, MG, and MGCNTs.
Sample 2	Control (L^+)	Bacterial samples were irradiated in the absence CNTs, MG, and MGCNTs for 3 mins.
Sample 3	CNT (L^-)	Bacterial samples treated with CNTs and incubated in the dark.
Sample 4	CNT (L^+)	Bacterial samples treated with CNTs and irradiated with 660 nm light for 3 mins.
Sample 5	MG (L^-)	Bacterial samples treated with MG and incubated in the dark.
Sample 6	MG (L^+)	Bacterial samples treated with MG and irradiated for 3 mins.
Sample 7	MGCNT (L^-)	Bacterial samples treated with MGCNTs and incubated in the dark.
Sample 8	MGCNT (L^+)	Bacterial samples treated with MGCNTs and irradiated for 3 mins.

the fluorescent product 2, 7-dichlorofluorescein (DCFH) after reacting with ROS. The fluorescence produced was measured using spectroscopic methods. Overnight test bacterial cultures were treated with CNTs, MG, and MGCNTs and pre-incubated for 3 hrs in dark. Unbound dye was removed from the samples by gentle washing with sterile PBS after incubation. The collected pellets were resuspended in sterile PBS and treated with 5 mM of DCFH-DA for 10 mins. The samples were irradiated for 3 mins after removing excess DCFH-DA. The DCF fluorescence produced was measured spectrophotometrically with an excitation wavelength of 495 nm and an emission wavelength of 529 nm.

Protein leakage and lipid peroxidation assay

Protein leakage was investigated using standard Bradford's protein estimation method.[25] All samples were centrifuged for 5 mins at 10,000 rpm. The optical density of the supernatant treated with Bradford's reagent was measured at 595 nm. A positive sample was prepared by treating the bacterial culture with cetyltrimethylammonium bromide (10 μg/mL). Protein leakage from cells after aPDT was calculated and compared with the cytoplasmic leakage index.

The lipid peroxides formed after aPDT were measured using thiobarbituric acid.[26] Lipid peroxides produced during oxidative stress induced by aPDT can be further oxidized to malondialdehyde (MDA) and 4-hydroxynonenal. Irradiated and non-irradiated samples were homogenized using 10% ice-cold trichloroacetate. The homogenate was collected after centrifuging for 15 mins at 14,000 rpm. Then, 1 mL of 2 thiobarbituric acid (0.6%) was added to the collected homogenate and the mixture held in boiling water for 10 mins. The chromogenic compound formed owing to the reaction between MDA and TBA was quantified spectrophotometrically at 535 nm. The lipid peroxide formation was measured by comparison with the MDA standards.

Biofilm inhibition assay

The inhibition in the biofilm formation after aPDT was assessed as follows.[27] After 24 hrs of incubation, the samples were diluted 10 fold in LB broth and incubated at 37°C for 24 hrs. The free floating cells from the wells were removed by gentle washing with PBS and held for 2 mins for drying. The biofilms formed in the wells were stained with 200 μL of 0.1% crystal violet and incubated for 15 mins at room temperature. The excess crystal violet was removed. Dye bound to the biofilm was eluted with 95% ethanol (100 μL). The inhibition in biofilm formation was determined by measuring optical density at 570 nm. The reduction in the formation of biofilm was measured using the formula:

$$\%\ Biofilm\ inhibition = [(OD_{570}\ of\ control - OD_{570}\ of\ test)/OD_{570}\ of\ control] * 100$$

Cell viability assay

2, 3, 5-Triphenyl tetrazolium chloride (TTC) was used to determine the cell viability after aPDT.[28] Samples after treatment were washed gently with sterile PBS. Approximately 100 μL of 0.5% of freshly prepared TTC was pipetted into each well after 24 hrs of incubation. The experimental setup was incubated for 5 mins at room temperature. The reduction in the viability of cells after irradiation was measured spectrophotometrically at 485 nm.

Quantification of EPS

Congo red dye was used for the quantification of produced EPS in biofilms.[29] Overnight bacterial cultures (100 μL) were treated with CNT, MG, and MGCNT as described above. After irradiation, the samples were allowed to grow to brain heart infusion broth (BHI) comprised of 1% sucrose and incubated at 37°C for 24 hrs. After incubation, the broth was removed and Congo red (50 μL, 50 mM) was added to the wells along with the fresh medium. Blank wells having only Congo red were maintained as a control. The above mixture was centrifuged for 5 mins at 10,000 rpm after an incubation period of 2 hrs at room temperature. The reduction in the EPS was determined by measuring the absorbance of the supernatant at 490 nm. EPS reduction was measured by comparing the optical density of treated samples with that of blank Congo red.

Live and dead cell assay

To study the effect of aPDT, the biofilms of bacteria were visualized under confocal laser scanning microscopy (CLSM) (LSM710, Carl Zeiss, Germany). Bacterial test strains were allowed to grow on a cover slip placed in wells containing BHI broth (1% sucrose) with and without compounds. The samples were pre-incubated for 3 hrs in the dark and then irradiated for 3 mins as described previously. The samples were then incubated at 37°C for 48 hrs. The free floating cells were removed from the cover slips by gentle washing with sterile PBS. The biofilm developed on the cover slip was stained with ethidium

bromide and acridine orange dye (100 µL) and held at 37°C for 15 mins. The excess dye was removed, and the cover slips viewed under CLSM.

Statistical analysis

All results are presented with their respective mean and standard deviations of triplicate experiments. Values were compared and analyzed along with their controls. One way analysis of variance was used to test the statistical significance among the data when *P*-values were ≤0.001. Asterisks (***) indicate the statically significant groups.

Results

Characterization of the MGCNT conjugate

The optical properties analyzed via UV-visible spectroscopy revealed the maximum absorbance of CNTs and MG at 268 and 614 nm, respectively (Figure 1A). The strong absorbance bands of CNTs correspond to their surface plasmon resonance. The MGCNT conjugate exhibited two characteristic absorbance bands at 270 and 618 nm that indicate the presence of both MG and CNTs in the conjugate. The HRTEM micrograph (Figure 1B) revealed the size of synthesized MGCNTs as 10 nm. The MGCNT conjugate was observed without aggregates indicating the uniform attachment of dye to the CNTs. The functional groups of CNTs, MG, and MGCNTs were graphed between a range of 450–4000 cm^{-1}. The functional groups of CNTs were observed at 1,069.30, 1,455.18, 2,362.01, and 3,404.96 cm^{-1}. The characteristic O–H stretching, carboxyl, and carbonyl C–O stretching, O–H deformations, and C–O stretching of CNTs corresponded to 3404.96, 1455.18, and 1069.30 cm^{-1}, respectively. MG revealed characteristic peaks at 1,172.52, 1,381.62, 16,563.73, and 3,440 cm^{-1}, which correspond to the various monosubstituted and paradisubstituted benzene rings. The peaks at 1,172.52 and 1,563.73 cm^{-1} correspond to the C–N stretching of benzene and C=C stretching of the benzene ring. The presence of infrared bands in MGCNTs at 1,095.03, 1,641.69, 2,920.47, and 3442.48 cm^{-1} corresponded to both CNTs and MG, which confirmed the conjugation process (Figure 2A).

LC of MG and EE of CNTs

High loading of MG and entrapment efficacy of CNTs were observed, which resulted in the improved aPDT. The amount of MG bound to the CNTs was measured as 10.31±0.77%. The EE of CNTs was 82.51±6.20%.

In vitro release of MG

The amount of dye released from the CNTs reached a maximum at 180 mins, being recorded as 26.24±1.30%

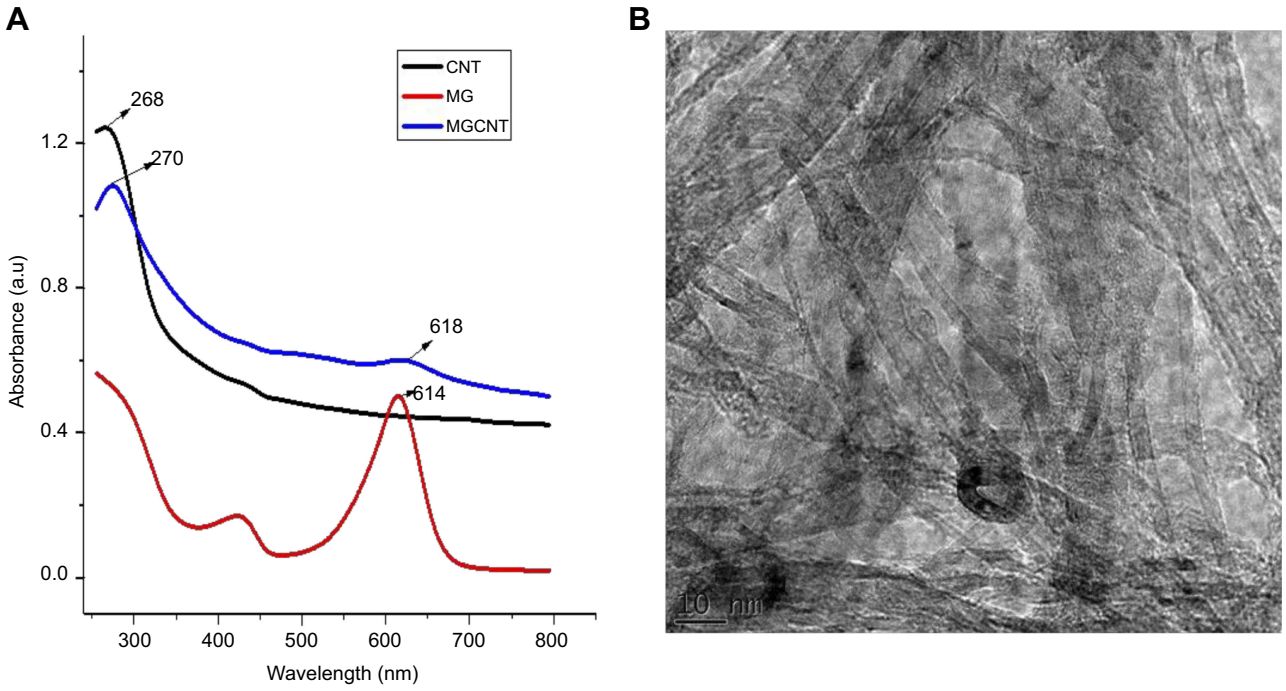

Figure 1 (**A**) UV–vis absorbance spectra of CNTs, MG, and MGCNTs. (**B**) HRTEM micrograph of MGCNTs.

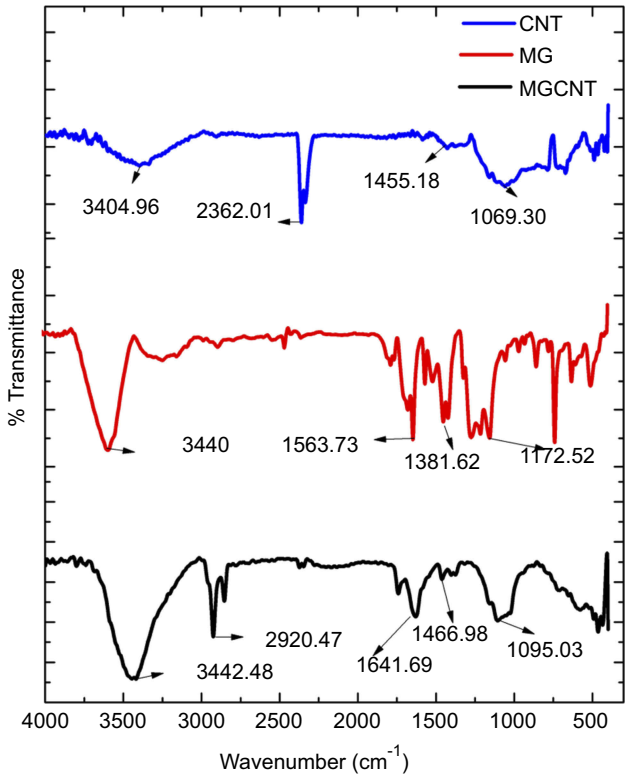

Figure 2 FTIR spectral analysis for the functional groups present in the CNTs, MG, and MGCNTs.

(Figure 3A). Statistical analysis of the release kinetics of MG from MGCNTs was investigated by fitting the in vitro release data to a Korsmeyer–Peppas model. The analysis calculated the coefficient (R^2) of the linear relationship between MG release and time that was established upon fitting to the Koermeyer–Peppas model. The kinetic parameters observed are shown in Table 2.

Uptake of MG by bacteria

The maximum uptake of MGCNTs and MG by *S. aureus* was 39.41±1.92% and 19.41±0.62%, respectively, at 150 mins (Figures 3B and C). The maximum uptake of MGCNTs and MG by *P. aeruginosa* was also recorded at 150 mins, being 29.87±1.42% and 19.87±1.28%.

Antimicrobial photodynamic inactivation of planktonic bacteria

The photoinactivation of *S. aureus* and *P. aeruginosa* using MGCNTs with an exposure time of 3 mins yielded a significant 5.55 and 5.16 $\log_{10}$ reduction, respectively (Figure 3D). The photoinactivation results of different exposure times (5 and 10 mins) are given in the supplementary file (Table S1). The phototoxicity of MG and CNTs on both test organisms was less compared to that from the treatment with the MGCNT conjugate. Treatment with MG showed a reduction in the growth of *S. aureus* cells by 2.83 $\log_{10}$ reduction after being photoactivated by light compared to 2.16 $\log_{10}$ reduction in *P. aeruginosa*. The $\log_{10}$ reductions in non-irradiated and irradiated test cultures (control) were less significant when compared to the phototoxicity exhibited by the MGCNT conjugate.

Determination of ROS

The amount of ROS produced through aPDT was measured in irradiated and non-irradiated samples along with controls. The amount of ROS produced correlated with the DCF fluorescence intensity measured in treated samples, which was high in MGCNT-treated *S. aureus* and *P. aeruginosa* but very low in the controls for both test bacteria. Overall, MGCNT-treated samples exhibited high DCF fluorescence intensity compared to that of CNT or MG-treated and non-irradiated samples (Figure 4A).

Protein leakage and lipid peroxidation assay

The percentage of protein leakage after treatment with MGCNTs was 46.79±1.38% in *P. aeruginosa* and 53.68 ±1.35% in *S. aureus*. Protein leakage in test bacteria in the presence of CNTs and MG was less compared to that with the MGCNT conjugate, indicating a greater degree of cell membrane damage owing to the conjugate (Figure 4B). The amount of lipid peroxide produced was greater in MGCNT-treated compared with MG-treated samples and was very low in control samples without irradiation. The amount of MDA produced after aPDT in *S. aureus* and *P. aeruginosa* was 12.31 ±0.62 and 11.96±1.11 nM/mL, respectively (Figure 4C).

Assessment of anti-biofilm activity of MGCNTs

MG and MGNT treatment resulted in reduced biofilm formation in *S. aureus* of 41.04±1.11 and 67.59±3.53%, whereas in *P. aeruginosa* the amount of biofilm reduction was 25.70±1.13 and 60.20±2.48% in MG and MGCNT-treated samples (Figure 4D). Biofilm formation was not reduced in the control (culture) when compared to that in the treated samples. The amount of TTC bound to the cells is a direct measure of the metabolic activity of biofilms. The reduction in the viability of *S. aureus* after treatment with MG and MGCNTs was 43.57 ±1.43% and 62.54±3.00%, whereas it was 29.42±1.06% and 61.53±3.86% in *P. aeruginosa*, respectively (Figure 5A).

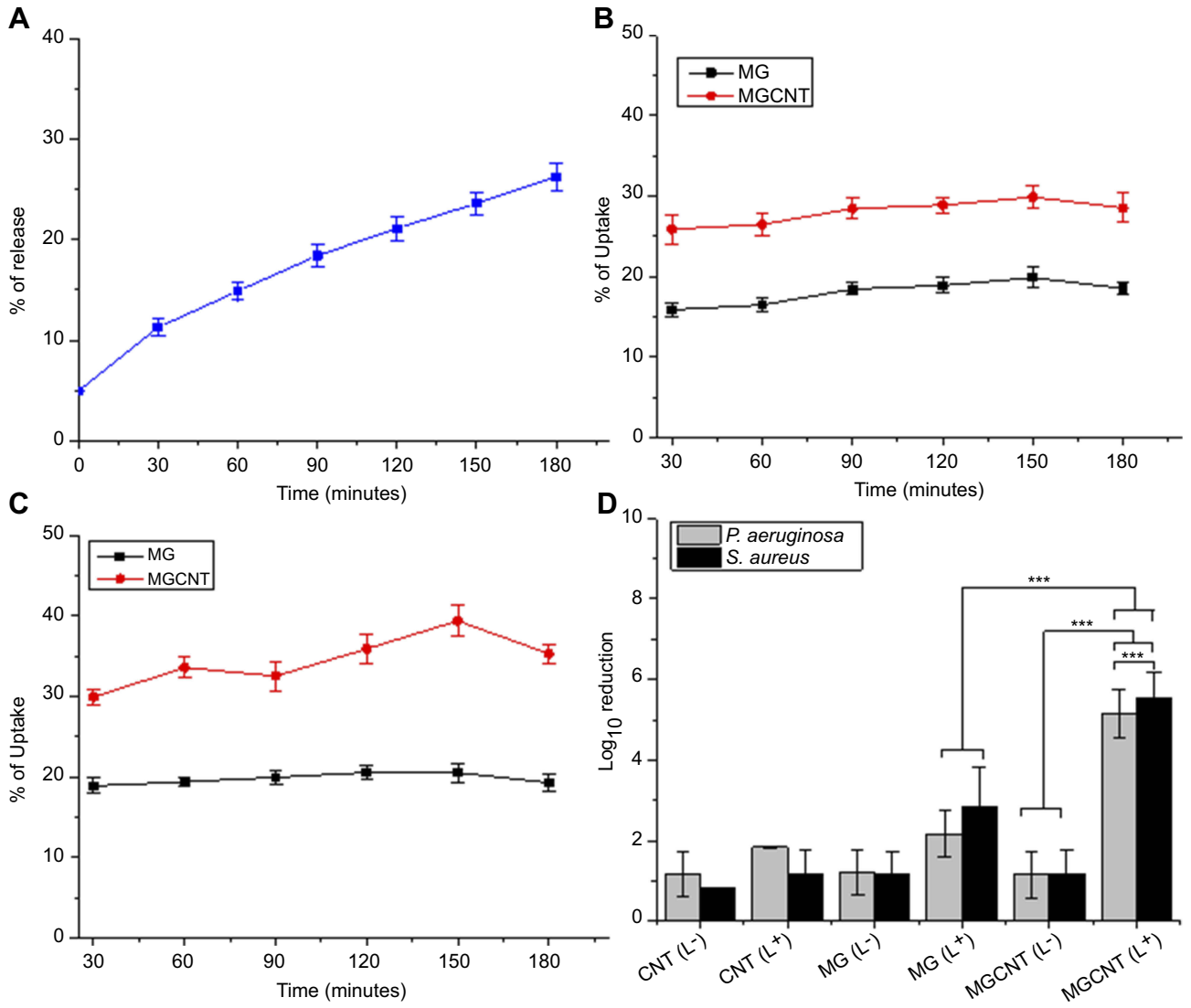

Figure 3 (**A**) Release of malachite green from CNTs at 37°C and pH 7.4. Uptake of malachite green and MGCNTs by (**B**) *P. aeruginosa* and (**C**) *S. aureus*. (**D**) The $\log_{10}$ reductions of *P. aeruginosa* and *S. aureus* after treatment with CNTs, MG, and MGCNTs. Non-irradiated and irradiated cells are represented by (L^-) and (L^+), respectively. Asterisks (***) represent the statistical significance between the respective dark control and the free dye and nanocomposite (*P*-value <0.001).

Table 2 MG release kinetics and correlation coefficient values from the Korsmeyer–Pappas kinetics model

Kinetic parameter	Value
Kinetic constant (*K*)	1.9806
Release exponent (*n*)	0.4931
Correlation coefficient (R^2)	0.9995

A more substantial reduction in EPS production was found in MGCNT-treated cells of *S. aureus* and *P. aeruginosa* when compared to that from the dark incubation. The amount of EPS reduction was 27.12 ±1.63% and 57.84±1.82% in MG and MGCNT-treated samples of *S. aureus*. In *P. aeruginosa*, the level of EPS inhibition was 19.89±1.46% and 37.25±1.50% for MG and MGCNT-treatment (Figure 5B).

CLSM analysis

CLSM analysis revealed the presence of green fluorescence, which indicated live cells in the control group. MG and MGCNT-treated cells of both test bacteria exhibited more red fluorescence, indicative of dead cells. Biofilms of *S. aureus* and *P. aeruginosa* treated with MG showed both live and dead cells whereas MGCNT-treated biofilms were observed to contain more dead cells (Figure 6). The non-irradiated samples revealed more live cells in comparison to the irradiated samples. These results confirmed a greater

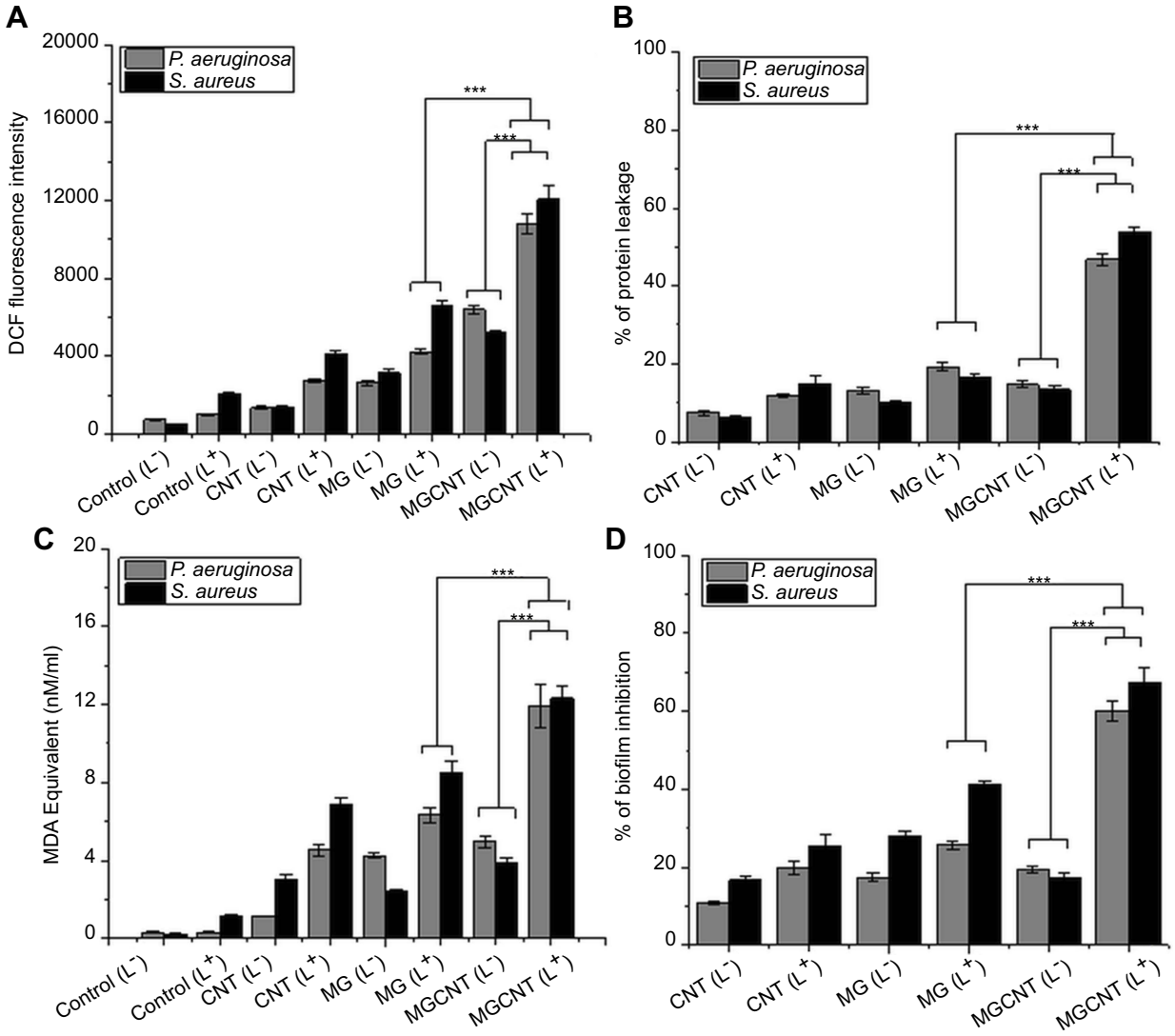

Figure 4 (**A**) Total reactive oxygen species produced in *P. aeruginosa* and *S. aureus* after photoinactivation. (**B**) Percentage of protein leakage from cells after aPDT. (**C**) Lipid peroxides formed in *P. aeruginosa* and *S. aureus* after aPDT. (**D**) Inhibition of biofilms of *P. aeruginosa* and *S. aureus*. Non-irradiated and irradiated cells are represented by (L^-) and (L^+), respectively. Asterisks (***) represent the statistical significance between the respective dark control and the free dye and nanocomposite (*P*-value<0.001).

level of photodestruction in MGCNT-treated samples compared to that following MG treatment.

Discussion

In association with biofilms, *P. aeruginosa* and *S. aureus* exhibit increased resistance to conventional antibiotics and are most frequently linked to health care-associated infections.[30,31] The failure to eradicate such medical device and surgical site-associated biofilm infections, major causes of morbidity and mortality worldwide, through systemic antibiotic treatment has led to the development of alternative therapeutic methods.[1] Notably, aPDT constitutes an upcoming treatment modality that never leads to the development of resistance among bacterial strains. In turn, aPDT is not affected by various resistance mechanisms of bacteria as the phototoxicity is mediated by the production of ROS.[32] To efficiently implement such methodologies, there is an increased need for novel anti-biofilm agents that will prevent the adhesion of microorganisms, colonization, and biofilm formation on surfaces.[33] In the present study, we synthesized nanoconjugates using a cationic photosensitizer, MG, which exhibited high phototoxicity in *P. aeruginosa* and *S. aureus* biofilms.

The primary focus of this study was to evaluate and compare the anti-biofilm and antibacterial activity of MGCNTs on the bacterial strains *S. aureus* and *P. aeruginosa*. Although

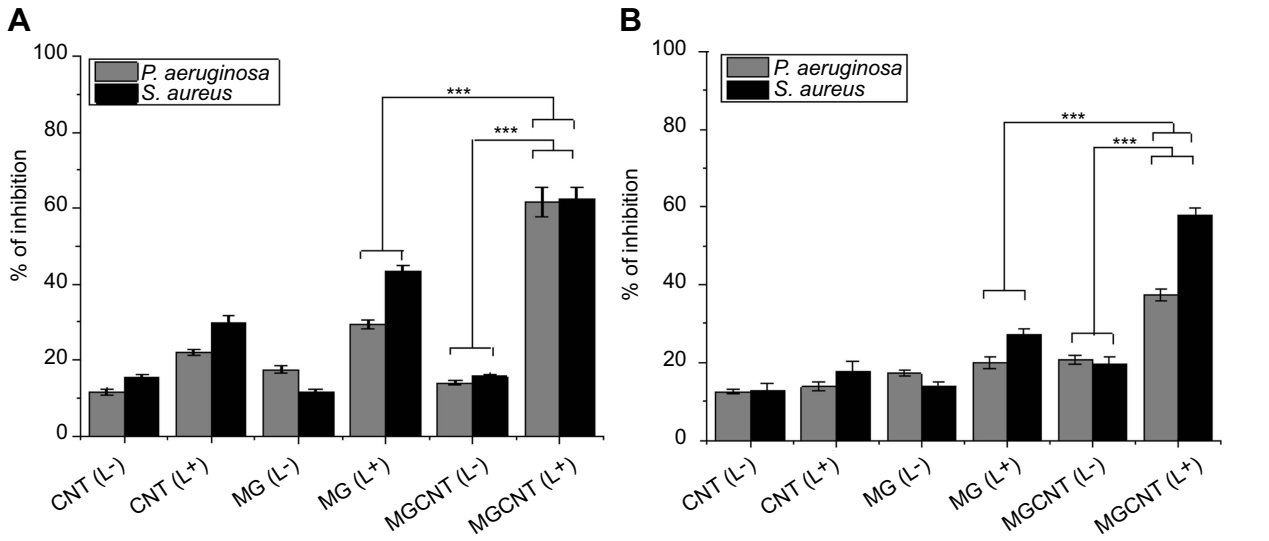

Figure 5 (**A**) Reduction in the cell viability of *P. aeruginosa* and *S. aureus* after aPDT treatment. (**B**) Reduction in exopolysaccharides of *P. aeruginosa* and *S. aureus* after aPDT. Non-irradiated and irradiated cells are represented by (L^-) and (L^+), respectively. Asterisks (***) represent the statistical significance between the respective dark control and the free dye and nanocomposite (*P*-value <0.001).

previous studies have described MG-mediated photodestruction among different organisms,[10] to our knowledge, the present study constitutes the first report of conjugation of the dye to a nanocarrier for enhanced photokilling. For example, a previous study found that 0.01% MG yielded a reduction in bacterial CFU of 99%.[34] Additionally, MG affords a significant reduction in *S. aureus* following treatment with 0.1 mg/mL of dye and irradiated with a 660 nm laser for 5 mins.[11] In turn, the surface modifications of CNTs exert considerable influence on the adsorption of dyes.[35] Numerous studies have revealed that CNTs exhibit higher adsorption efficiency to various synthetic dyes such as MG. In this study, the characterization of synthesized MGCNTs was performed using UV-visible spectroscopy, HRTEM, FTIR, and photoluminescence spectroscopy based on published methodologies.[36–38] Optical studies revealed that both MG and CNTs were present in the MGCNT conjugate as confirmed by the presence of absorption peaks for each in the conjugates.[39,40] Successful conjugation of the dye to the CNTs was confirmed by the absorbance studies along with HRTEM, FTIR, and photoluminescence. Together, these analyses provided considerable information regarding the interactions of MG with CNTs.

An advantage of conjugating a cationic dye to the nanocarrier is to permit the internalization and interaction of PS with the bacterial system, thereby mediating enhanced photodestruction at a lower concentration of dye. Moreover, Gram-negative bacteria are known to be susceptible toward aPDT as compared to Gram-positive bacteria as the highly developed and complex cell wall structure of Gram-positive bacteria renders them more permeable to PS than Gram-negative bacteria.[10] Nevertheless, the present study demonstrated the successful attachment and uptake of dye by both types of bacteria followed by their photoinactivation using ROS.[27] Specifically, the EE of the nanocarrier and loading of the dye comprise important parameters to achieve effective aPDT.[41] In the present study, we formulated a nanodye conjugate with good loading and EE for the effective and successful delivery of MG.

aPDT regimes are also significantly affected by the release properties of the dye from the nanocomposite and its binding and uptake by the bacterial system. In the present study, sustained release of MG occurred within 3 hrs and a release of 26.24% was achieved. This enabled the repeated exposure to PDT after a single administration of conjugate to the target, as MG shows a sustained release profile. A sustained and controlled release of cationic dye from the nanocomposite was similarly recorded in earlier studies.[20] The continuous and fast release profile of MG from the nanocarriers suggested the physical and supramolecular adsorption of dye to the CNTs. Overall, the results of the uptake and release study substantiate the primary goal of the present study to enhance the photodynamic inactivation abilities of MG against the test bacteria through conjugation with a nanocarrier.

Binding of MG to Gram-negative and -positive bacteria differs slightly depending on the charge of MG and the cell wall structure of the bacteria. The fraction of MG bound to

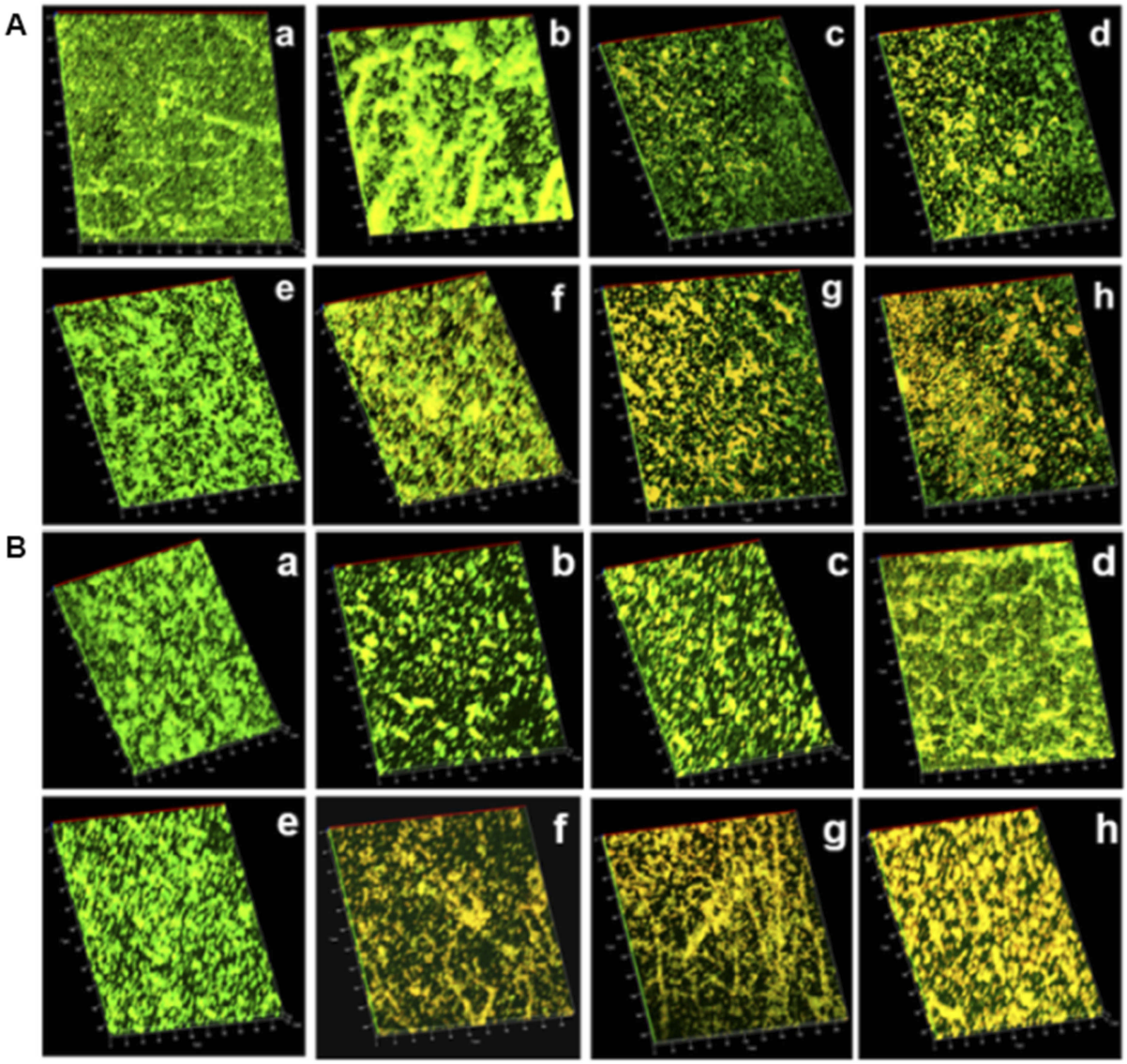

Figure 6 Confocal laser scanning microscopy images of biofilms of (**A**) *P. aeruginosa* and (**B**) *S. aureus*. (a) and (e) comprise non-irradiated and irradiated biofilms; (b) (c), and (d) are biofilms incubated in the dark and treated with CNTs, MG, and MGCNT, respectively; (f), (g), and (h) comprise biofilms treated with CNTs, MG, and MGCNTs, respectively, and irradiated.

the bacteria has been observed to be larger in samples treated with the nanoconjugate compared to the free dye.[29] aPDT using MG against Gram-positive and -negative bacteria was reported previously by employing a light of 660 nm for 4.45 mins.[10] Specifically, enhanced photoinactivation was observed in Gram positive compared to Gram-negative bacteria, with 7 $\log_{10}$ and 6 $\log_{10}$ reductions of *S. aureus* and *E. coli* detected following PDT with a high concentration of MG (0.1%) and longer light exposure time (5 mins).[10] In another study, MG-mediated aPDT resulted in 3.84 and 1.92 $\log_{10}$ reductions in *S. aureus* and *E. coli*, respectively.[42] MG at a concentration of 0.01% yielded a 3 $\log_{10}$ reduction of *Actinobacillus actinomycetemcomitans*. The photobactericidal mechanism of MG primarily relies upon type 1 mechanisms involving the production of hydroxyl anion, superoxide, and other oxygen free radicals.[34]

Previously, CNTs were used for conjugating methylene blue dye, which exhibited enhanced phototoxicity against *E. coli* and *S. aureus*. The ability of CNTs to act as a dye delivery vehicle to bacterial systems for enhanced antibacterial was confirmed.[23] In the present study, both bacterial strains were more sensitive to the MGCNT-mediated killing than that of free dye and CNTs, validating the ability of CNTs to carry MG and exhibit pronounced phototoxicity against test bacteria. The slightly greater phototoxicity observed in *S. aureus* was correlated to the quantity of

ROS produced. The photo-mediated generation of ROS occurs in bacteria as cationic dyes easily bind and diffuse to the cell membrane. This leads to an alteration in the integrity of the cell membrane and eventually to the leakage of essential components and cell death.[43]

The photoinactivation ability of the conjugate on the bacterial biofilm was also determined. Biofilm formation was inhibited significantly, indicating the efficacy of the MGCNT conjugate toward biofilm and planktonic cells. This clearly suggested that the dye was able to penetrate deeper layers of the biofilm.[27] The metabolic activity or viability was also more severely affected by the MGCNT conjugate than free dye treatment. This may be due to the inhibitory action of the MGCNT conjugate against the developmental stages of the biofilm. The significant EPS reduction in MGCNT-treated cells compared to the control provided support for the disruption of biofilm architecture. A high degree of biofilm reduction was detected in MGCNT-treated cells of *S. aureus* and *P. aeruginosa* compared to that in the control samples, which was further confirmed with CLSM analysis.[44] The results thus indicated that the MGCNT conjugate could be used as an alternative approach for the prevention and treatment of infections caused by *P. aeruginosa* and *S. aureus* biofilms.

Conclusion

The field of nanotechnology has become an integral part of medicine with wide applications in drug delivery methods. As an emerging drug delivery agent, CNTs have recently gained additional interest as attractive scaffolds in antimicrobial therapy for drug carriers. The present findings demonstrated the improved efficiency of aphotoactivated MGCNT conjugate for antimicrobial therapy against *S. aureus* and *P. aeruginosa*. The ability of the MGCNT conjugate to potentiate antimicrobial photodynamic inactivation against the test bacteria provides valuable information that may contribute to the design of efficient and potent antimicrobial and anti-biofilm agents. Moreover, the conjugate was able to reduce the planktonic cells along with biofilms of both *P. aeruginosa* and *S. aureus*. These findings suggested that, aPDT using the MGCNT conjugate might be employed as an alternative approach for the elimination of both forms of these bacteria from medical devices.

Acknowledgments

The authors extend their appreciation to the Deanship of Scientific Research at King Saud University for funding this work through research group No (RG-1440-053). We sincerely acknowledge the support received from Department of Physics (Pondicherry University), Central Instrumentation Facility (Pondicherry University) and iThemba LABS-National Research Foundation (NRF), Somerset West, Western Cape Province, South Africa to complete the research work. The authors are also thankful to Bharathidasan University, Tiruchirappalli for providing access to the Confocal Laser Scanning Microscopy.

Disclosure

The authors report no conflicts of interest in this work.

References

1. Bayramov DF, Neff JA. Beyond conventional antibiotics – new directions for combination products to combat biofilm. *Adv Drug Deliv Rev*. 2017;112:48–60. doi:10.1016/j.addr.2016.07.010
2. Percival SL, Suleman L, Vuotto C, Donelli G. Healthcare-associated infections, medical devices and biofilms: risk, tolerance and control. *J Med Microbiol*. 2015;64(Pt 4):323–334. doi:10.1099/jmm.0.000032
3. Sommer R, Joachim I, Wagner S, Titz A. New approaches to control infections: anti-biofilm strategies against gram-negative bacteria. *Chimia (Aarau)*. 2013;67(4):286–290. doi:10.2533/chimia.2013.286
4. Campoccia D, Montanaro L, Arciola CR. The significance of infection related to orthopedic devices and issues of antibiotic resistance. *Biomaterials*. 2006;27(11):2331–2339. doi:10.1016/j.biomaterials.2005.11.044
5. Zhang R, Eggleston K, Rotimi V, Zeckhauser RJ. Globalization and health antibiotic resistance as a global threat : evidence from China, Kuwait and the United States. *Global Health*. 2006;2:6. doi:10.1186/1744-8603-2-6
6. Paraje MG. Antimicrobial resistance in biofilms. In: Méndez-Vilas A, editor. *Science against Microbial Pathogens: Communicating Current Research Technological Advances*. Vol. 2. Formatex Research Center, Badajoz, Spain: 2011;736–744.
7. Briggs T, Blunn G, Hislop S, et al. Antimicrobial photodynamic therapy – a promising treatment for prosthetic joint infections. *Lasers Med Sci*. 2018;33(3):523–532. doi:10.1007/s10103-017-2394-4
8. Hu X, Huang Y, Wang Y, Wang X, Hamblin MR. Antimicrobial photodynamic therapy to control clinically relevant biofilm infections. *Front Microbiol* 2018;9:1299. doi:10.3389/fmicb.2018.01299
9. Rosa LP, Da Silva FC. Antimicrobial photodynamic therapy: a new therapeutic option to combat infections. *J Med Microb Diagn*. 2014;3:158. doi:10.4172/2161-0703.1000158
10. Junqueira JC, Ribeiro MA, Rossoni RD, Barbosa JO, Querido SMR, Jorge AOC. Antimicrobial photodynamic therapy: photodynamic antimicrobial effects of malachite green on *Staphylococcus*, Enterobacteriaceae, and *Candida*. *Photomed Laser Surg*. 2010;28(Suppl 1):S67–S72. doi:10.1089/pho.2009.2526
11. Rosa LP, Da Silva FC, Nader SA, Meira GA, Viana MS. Antimicrobial photodynamic inactivation of *Staphylococcus aureus* biofilms in bone specimens using methylene blue, toluidine blue ortho and malachite green: an in vitro study. *Arch Oral Biol*. 2015;60(5):675–680. doi:10.1016/j.archoralbio.2015.02.010
12. Huang YY, Sharma SK, Dai T, et al. Can nanotechnology potentiate photodynamic therapy? *Nanotechnol Rev*. 2012;1(2):111–146. doi:10.1515/ntrev-2011-0005
13. Cavallaro G, Lazzara G, Milioto S, et al. Nanohydrogel formation within the halloysite lumen for triggered and sustained release. *ACS Appl Mater Interfaces*. 2018;10(9):8265–8273. doi:10.1021/acsami.7b19361

14. Makaremi M, Pasbakhsh P, Cavallaro G, et al. Effect of morphology and size of halloysite nanotubes on functional pectin bionanocomposites for food packaging applications. *ACS Appl Mater Interfaces*. 2017;9(20):17476–17488. doi:10.1021/acsami.7b04297
15. Al-Jumaili A, Alancherry S, Bazaka K, Jacob M. Review on the antimicrobial properties of carbon nanostructures. *Materials (Basel)*. 2017;10(9):E1066. doi:10.3390/ma10091066
16. Banerjee I, Mondal D, Martin J, Kane RS. Photoactivated antimicrobial activity of carbon nanotube - porphyrin conjugates. *Langmuir*. 2010;26(22):17369–17374. doi:10.1021/la103298e
17. Meng L, Zhang X, Lu Q, Fei Z, Dyson PJ. Single walled carbon nanotubes as drug delivery vehicles: targeting doxorubicin to tumors. *Biomaterials*. 2012;33(6):1689–1698. doi:10.1016/j.biomaterials.2011.11.004
18. Vt A, Paramanantham P, Sl S, et al. Antimicrobial photodynamic activity of rose bengal conjugated multi walled carbon nanotubes against planktonic cells and biofilm of *Escherichia coli*. *Photodiagnosis Photodyn Ther*. 2018;24:300–310. doi:10.1016/j.pdpdt.2018.10.013
19. Sah U, Sharma K, Chaudhri N, Sankar M, Gopinath P. Antimicrobial photodynamic therapy: single-walled carbon nanotube (SWCNT)-Porphyrin conjugate for visible light mediated inactivation of *Staphylococcus aureus*. *Colloids Surf B Biointerfaces*. 2018;162:108–117. doi:10.1016/j.colsurfb.2017.11.046
20. Usacheva M, Layek B, Nirzhor SS, Prabha S. Nanoparticle-mediated photodynamic therapy for mixed biofilms. *J Nanomater*. 2016;2016:1–11. doi:10.1155/2016/4752894
21. Shrestha A, Kishen A. Polycationic chitosan-conjugated photosensitizer for antibacterial photodynamic therapy. *Photochem Photobiol*. 2012;88(3):577–583. doi:10.1111/j.1751-1097.2011.01026.x
22. Rosa LP, Da Silva FC, Nader SA, Meira GA, Viana MS. In vitro effectiveness of antimicrobial photodynamic therapy (APDT) using a 660 nm laser and malachite green dye in *Staphylococcus aureus* biofilms arranged on compact and cancellous bone specimens. *Lasers Med Sci*. 2014;29(6):1959–1965. doi:10.1007/s10103-014-1613-5
23. Parasuraman P, Anju VT, Sruthil Lal SB, et al. Synthesis and antimicrobial photodynamic effect of methylene blue conjugated carbon nanotubes on *E. coli* and *S. aureus*. *Photochem Photobiol Sci*. 2019;18(2):563–576. doi:10.1039/c8pp00369f
24. Garcez AS, Núñez SC, Baptista MS, et al. Antimicrobial mechanisms behind photodynamic effect in the presence of hydrogen peroxide. *Photochem Photobiol*. 2012;10(4):483–490. doi:10.1039/c0pp00082e
25. Singh M, Mallick AK, Banerjee M, Kumar R. Loss of outer membrane integrity in gram-negative bacteria by silver nanoparticles loaded with *Camellia sinensis* leaf phytochemicals: plausible mechanism of bacterial cell disintegration. *Bull Mater Sci*. 2016;39 (7):1871–1878. doi:10.1007/s12034-016-1317-5
26. Sheng H, Nakamura K, Kanno T, Sasaki K, Niwano Y, Wu M. Bactericidal effect of photolysis of H2O2 in combination with sonolysis of water via hydroxyl radical generation. *PLoS One*. 2015;10(7): e0132445. doi:10.1371/journal.pone.0132445
27. Misba L, Kulshrestha S, Khan AU. Antibiofilm action of a toluidine blue O-silver nanoparticle conjugate on *Streptococcus mutans* : a mechanism of type I photodynamic therapy. *Biofouling*. 2016;32 (3):313–328. doi:10.1080/08927014.2016.1141899
28. Moussa SH, Tayel AA, Al-Hassan AA, Farouk A. Tetrazolium/formazan test as an efficient method to determine fungal chitosan antimicrobial activity. *J Mycol*. 2013;2013:1–7. doi:10.1155/2013/753692
29. Misba L, Zaidi S, Khan AU. A comparison of antibacterial and antibiofilm efficacy of phenothiazinium dyes between gram positive and gram negative bacterial biofilm. *Photodiagnosis Photodyn Ther*. 2017;18:24–33. doi:10.1016/j.pdpdt.2017.01.177
30. Percival SL, Hill KE, Williams DW, Hooper SJ, Thomas DW, Costerton JW. A review of the scientific evidence for biofilms in wounds. *Wound Repair Regen*. 2012;20(5):647–657. doi:10.1111/j.1524-475X.2012.00836.x
31. Seth AK, Geringer MR, Hong SJ, Leung KP, Mustoe TA, Galiano RD. In vivo modeling of biofilm-infected wounds: A review. *J Surg Res*. 2012;178(1):330–338. doi:10.1016/j.jss.2012.06.048
32. St. Denis TG, Dai T, Izikson L, et al. All you need is light. *Virulence*. 2011;2(6):509–520. doi:10.4161/viru.2.6.17889
33. Francolini I, Donelli G. Prevention and control of biofilm-based medical-device-related infections. *FEMS Immunol Med Microbiol*. 2010;59(3):227–238. doi:10.1111/j.1574-695X.2010.00665.x
34. Prates RA, Yamada AM Jr, Suzuki LC, et al. Bactericidal effect of malachite green and red laser on *Actinobacillus actinomycetemcomitans*. *J Photochem Photobiol B Biol*. 2006;86 (1):70–76. doi:10.1016/j.jphotobiol.2006.07.010
35. Zare K, Gupta VK, Moradi O, et al. A comparative study on the basis of adsorption capacity between CNTs and activated carbon as adsorbents for removal of noxious synthetic dyes: a review. *J Nanostructure Chem*. 2015;5(2):227–236. doi:10.1007/s40097-015-0158-x
36. Lehman JH, Terrones M, Mansfield E, Hurst KE, Meunier V. Evaluating the characteristics of multiwall carbon nanotubes. *Carbon N Y*. 2011;49 (8):2581–2602. doi:10.1016/j.carbon.2011.03.028
37. Zhang F, Chen X, Zhang W, Ji Y. Dual-functionalized strontium phosphate hybrid nanopowder for effective removal of Pb 2+ and malachite green from aqueous solution. *Powder Technol*. 2017;318:128–134. doi:10.1016/j.powtec.2017.05.031
38. Cheriaa J, Khaireddine M, Rouabhia M, Bakhrouf A. Removal of triphenylmethane dyes by bacterial consortium. *Sci World J*. 2012;2012:1–9. doi:10.1100/2012/512454
39. Mocan LT, Tabaran FA, Mocan T, et al. Selective ex-vivo photothermal ablation of human pancreatic cancer with albumin selective ex-vivo photothermal ablation of human pancreatic cancer with albumin functionalized multiwalled carbon nanotubes. *Int J Nanomed*. 2014; (April 2011)2011. 6: 915–928. doi:10.2147/IJN.S19013
40. Huang L, Weng X, Chen Z, Megharaj M, Naidu R. Synthesis of iron-based nanoparticles using oolong tea extract for the degradation of malachite green. *Spectrochim Acta Part A Mol Biomol Spectrosc*. 2014;117:801–804. doi:10.1016/j.saa.2013.09.054
41. Wallace SJ, Li J, Nation RL, Boyd BJ. Drug release from nanomedicines: selection of appropriate eEncapsulation and release methodology. *Drug Deliv Transl Res*. 2012;2(4):284–292. doi:10.1007/s13346-012-0064-4.Drug
42. Vilela SF, Junqueira JC, Barbosa JO, Majewski M, Munin E, Jorge AO. Photodynamic inactivation of *Staphylococcus aureus* and *Escherichia coli* biofilms by malachite green and phenothiazine dyes: an in vitro study. *Arch Oral Biol*. 2012;57(6):704–710. doi:10.1016/j.archoralbio.2011.12.002
43. Grinholc M, Nakonieczna J, Fila G, et al. Antimicrobial photodynamic therapy with fulleropyrrolidine: photoinactivation mechanism of *Staphylococcus aureus*, in vitro and in vivo studies. *Appl Microbiol Biotechnol*. 2015;99(9):4031–4043. doi:10.1007/s00253-015-6539-8
44. Khan S, Alam F, Azam A, Khan AU. Gold nanoparticles enhance methylene blue-induced photodynamic therapy: a novel therapeutic approach to inhibit *Candida albicans* biofilm. *Int J Nanomedicine*. 2012;7:3245–3257. doi:10.2147/IJN.S31

Supplementary material

Table S1 Antimicrobial photodynamic effect of MGCNT with different time periods of light irradiation

Time (min)	*Pseudomonas aeruginosa* (CFU/mL)				*Staphylococcus aureus* (CFU/mL)			
	Exp 1	Exp 2	Exp 3	Mean	Exp 1	Exp 2	Exp 3	Mean
0	7.9×10^7	7.6×10^7	8.2×10^7	7.9×10^7	1.2×10^8	8.9×10^7	7.8×10^7	9.5×10^7
3	3.5×10^2	4.3×10^2	3.2×10^2	3.6×10^2	3.2×10^2	2.9×10^2	3.5×10^2	3.2×10^2
5	5.1×10^2	6.0×10^2	4.3×10^2	3.8×10^2	3.0×10^2	2.9×10^2	3.4×10^2	3.1×10^2
10	3.9×10^2	4.8×10^2	4.1×10^2	4.2×10^2	3.3×10^2	3.1×10^2	3.2×10^2	3.2×10^2
15	4.1×10^2	3.5×10^2	4.3×10^2	3.9×10^2	3.4×10^2	3.7×10^2	3.0×10^2	3.3×10^2